Error propagation in two-sensor three-dimensional position estimation

John N. Sanders-Reed, MEMBER SPIE
Boeing-SVS, Inc.
4411 The 25 Way, Suite 350
Albuquerque, New Mexico 87109

Abstract. The accuracy of 3D position estimation using two angles-only sensors (such as passive optical imagers) is investigated. Beginning with the basic multisensor triangulation equations used to estimate a 3D target position, error propagation equations are derived by taking the appropriate partial derivatives with respect to various measurement errors. Next the concept of Gaussian measurement error is introduced and used to relate the standard deviation of various measurement errors to the standard deviation of the target 3D position estimate. Plots of the various error propagation coefficients are generated. These analytical results are verified using a Monte Carlo statistical approach. The result is a set of equations and graphs useful for designing a two-sensor system to meet a required accuracy specification. [DOI: 10.1117/1.1353798]

Subject terms: triangulation; 3D position estimation; angles only; multisensor; passive ranging; error propagation.

Paper 200065 received Feb. 22, 2000; revised manuscript received Sep. 11, 2000; accepted for publication Oct. 9, 2000.

1 Introduction

Passive, angles-only sensors are used in a number of fields, in different ways, to determine the 3D position of objects. These methods range from trilateration,[1–3] which uses the time of arrival of a unique signal from an object at multiple fixed sensors, to astronomical parallax measurements[4–7] to determine the distance of nearby astronomical objects from their apparent motion relative to distant objects as the observer (earth) moves, to triangulation. Triangulation can be performed using multiple sensors at known locations to determine the location of a fixed or moving object, or it can be performed using a moving sensor (observing a stationary target) to create a virtual baseline over time.[8–10] The technique of interest in this paper is triangulation between two sensors.

Triangulation between multiple sensors has been used in a number of fields, including particle-tracking velocimetry (PTV) for flow analysis,[11–18] surveillance,[19] range instrumentation,[20] obstacle avoidance,[21] and automotive crash test analysis. Surprisingly, despite the use of triangulation for 3D position (and hence velocity) estimation in these fields, there has been little analysis of error propagation and sensitivity published. The only substantial effort at error analysis in the PTV field was by Guezennec and Kiritsis,[18] in which they generated synthetic images with known particle properties, in order to perform a statistical test of their image-processing and triangulation algorithm. However, that work did not address errors in sensor position and orientation. Angus[19] provides a theoretical analysis of range errors (for a specific collinear three-sensor system) due to uncertainties in sensor azimuth angles, but assumes the sensor locations are known exactly and does not address elevation-angle errors. Sanders-Reed[20] investigated a three-sensor system with arbitrary sensor locations, but, like Guezennec and Kiritsis, assumed sensor location and pointing were known exactly, and focused instead on the image-processing and triangulation errors using synthetically generated imagery having a known truth location for targets. Sridhar and Suorsa[21] compare errors in range estimation for two-sensor triangulation with those for a single moving sensor using optical flow and object size change as the sensor approaches the object. For the triangulation they assume that the sensor location (baseline) is known accurately, and that measurement errors are present in the object location measurement within the image (corresponding to angular pointing errors).

The present work extends this previous work by developing an analytical relationship between measurement errors in sensor location (x,y,z) and line of sight (LOS) orientation (azimuth and elevation angles) and the resulting 3D position estimate of the target. Inherent in this analysis is an understanding of how the sensor-to-target orientation affects the accuracy of the ultimate target position estimation.

Typically, two or more sensors are placed at known locations (x,y,z) and are pointed in the general direction of the object that it is desired to measure. The pointing angles are usually azimuth and elevation, measured in a suitable reference frame, such as relative to north or some convenient laboratory frame. While the analysis in this paper is general (applies to radar, electro-optical, or even acoustic sensors), the most common sensor used for this application is an optical sensor using a rectangular focal plane array. Although a roll angle can be included for focal plane array sensors, usually the sensor focal plane array is aligned with the azimuth and elevation axes, so the roll angle is zero and can be ignored.

In general, the minimum number of angles-only sensors that can be used to triangulate the 3D position of an object is two. The exception is a stationary target that can be

observed at two different times by moving a single sensor, thus creating a synthetic baseline. While multiple (more than two) sensors can be used to perform the 3D triangulation, in the current paper we restrict our error analysis to the somewhat simpler case of only two sensors. This restriction is justified as allowing for the most commonly used geometry.

For a focal plane array sensor, triangulation is performed by taking an image of the object with each sensor. The object location in each image is computed, and the pointing angle to the object is determined. This is done using the *incremental field of view* (IFOV), which is the angular extent of each pixel, and the number of pixels between the target and the optical axis of the system. Thus if a sensor is aligned with an azimuth angle of 45 deg and the object is found to be 10 pixels to the right of the optical axis with an IFOV of 0.01 deg per pixel, then the LOS azimuth to the target is 45.1 deg. For the analysis in this paper, any errors in the IFOV, or in the detected target location on the focal plane, are considered part of the overall pointing angle.

Practical implementations must also deal with several other considerations, which are beyond the scope of this paper. One must either synchronize the frame times from multiple sensors, or extrapolate data from the sample times of one sensor to those of another sensor. For short-focal-length lenses, the conversion from focal plane pixel coordinates to LOS angular coordinates is complicated by geometric optical distortion. For the purposes of this paper, these can all be considered basic LOS measurement error without consideration of the origin of the error. However, for a practical experimenter, understanding and control of these errors can be critical.

The following sections will provide an overview of the basic triangulation theory, followed by a mathematical derivation of the error propagation equations. Next the assumption of measurement errors having a Gaussian statistical distribution is introduced. Error propagation coefficients are computed and plotted over a range of sensor-to-target orientations. Following a section in which graphs of the error-propagation coefficient are presented, Monte Carlo results are presented and shown to be in agreement with the graphs. Based on the error-propagation equations and graphs, experimental setup considerations are discussed.

2 Theory

2.1 *3D Position Estimation*

This section presents a brief summary of theory and notation for basic multisensor 3D triangulation. We use the coordinate system shown in Fig. 1, where the target location is shown with the subscript t and the sensors are shown with subscript i. A minimum of two sensors is required to produce a solution, and if more than two sensors are available, the problem is overconstrained and becomes a least-squares problem.

The target location is specified as (x_t, y_t, z_t). The sensors are specified by both their location and their pointing angles. The sensor location is (x_i, y_i, z_i), while the azimuth is θ_i and the elevation is φ_i. Azimuth is measured clockwise from the positive y axis and takes on values from 0 to 2π rad, while elevation is measured from the x-y plane and takes on values between $-\pi$ and $+\pi$. The x-y plane distance from sensor i to the target is r_i.

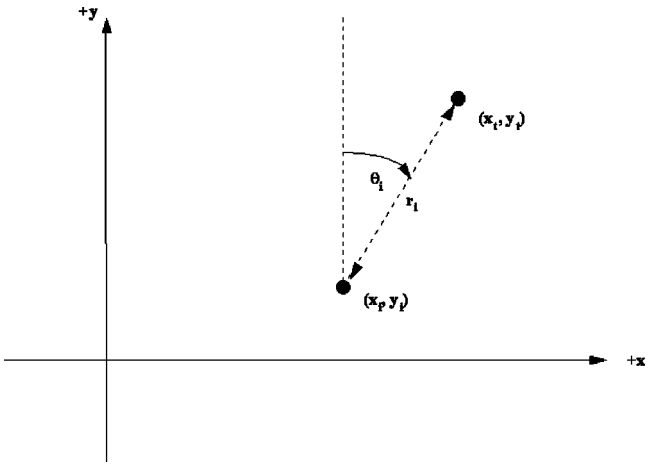

Fig. 1 3D triangulation coordinate system. Positive z axis is out of the paper.

The azimuth angle is related to the x-y plane coordinates of the target and sensor by

$$\tan\theta_i = \frac{x_t - x_i}{y_t - y_i}. \tag{1}$$

The target z location is related to the sensor z location, elevation angle, and x-y plane separation distance by

$$z_t = r_i \tan\varphi_i + z_i, \tag{2}$$

where

$$r_i = [(x_i - x_t)^2 + (y_i - y_t)^2]^{1/2}. \tag{3}$$

The general solution to Eq. (1), for N sensors, is a least-squares solution, best written in matrix notation as

$$\begin{bmatrix} \vdots \\ x_i - y_i \tan\theta_i \\ \vdots \end{bmatrix} = \begin{bmatrix} \vdots & \vdots \\ 1 & -\tan\theta_i \\ \vdots & \vdots \end{bmatrix} \begin{bmatrix} x_t \\ y_t \end{bmatrix}. \tag{4}$$

To compute z_t, we just compute the value for each sensor and average the values:

$$\langle z_t \rangle = \langle r_i \tan\varphi_i + z_i \rangle. \tag{5}$$

For a two-sensor problem, we can solve Eq. (1) explicitly, using subscripts 1 and 2 to denote the two sensors. In this case we arrive at

$$x_t = [x_2 \tan\theta_1 - x_1 \tan\theta_2 + (y_1 - y_2)\tan\theta_1 \tan\theta_2] \times (\tan\theta_1 - \tan\theta_2)^{-1}, \tag{6}$$

$$y_t = (y_1 \tan\theta_1 - y_2 \tan\theta_2 + x_2 - x_1)(\tan\theta_1 - \tan\theta_2)^{-1}. \tag{7}$$

Equations (6) and (7) are valid only for the two-sensor case. If one uses more than two sensors, Eq. (4) is the simplest solution for x_t and y_t.

2.2 *Error Propagation for Two Sensors*

In this section, we derive the error propagation equations for a two-sensor system. First we derive the basic error propagation equations giving the error in the final estimates of the target location for specific errors in the sensor position and pointing angles. Following this, we add the assumption of Gaussian random measurement errors.

To develop the relationship between the measurement error and the estimated value of x_t in Eq. (6), we perform a Taylor series expansion about the (unknown) true values, keeping only terms to first order, to write the error propagation equation for x_t:

$$\delta x_t \approx \frac{\partial x_t}{\partial x_1}\delta x_1 + \frac{\partial x_t}{\partial x_2}\delta x_2 + \frac{\partial x_t}{\partial y_1}\delta y_1 + \frac{\partial x_t}{\partial y_2}\delta y_2 + \frac{\partial x_t}{\partial \theta_1}\delta\theta_1 + \frac{\partial x_t}{\partial \theta_2}\delta\theta_2. \tag{8}$$

Assuming the errors are small, we have ignored higher-order terms. We call this the error propagation equation because, to first order, it describes the dependence of the final answer (e.g., x_t) on errors in each of the measured quantities. For example, to see how x_t varies with errors in the measurement of x_1 (the x position of sensor 1), we multiply the x_1 error estimate by the error coefficient, $\partial x_t/\partial x_1$. Looking at the results below, we see that the x_1 error coefficient depends on the separation angle between the two sensors ($\tan\theta_1 - \tan\theta_2$) and on $\tan\theta_2$.

The various partial derivatives in this equation are

$$\frac{\partial x_t}{\partial x_1} = -\frac{\tan\theta_2}{\tan\theta_1 - \tan\theta_2}, \qquad \frac{\partial x_t}{\partial x_2} = \frac{\tan\theta_1}{\tan\theta_1 - \tan\theta_2},$$

$$\frac{\partial x_t}{\partial y_1} = \frac{\tan\theta_1\tan\theta_2}{\tan\theta_1 - \tan\theta_2}, \qquad \frac{\partial x_t}{\partial y_2} = -\frac{\tan\theta_1\tan\theta_2}{\tan\theta_1 - \tan\theta_2},$$

$$\frac{\partial x_t}{\partial \theta_1} = \left[\frac{x_2 + (y_1 - y_2)\tan\theta_2}{\tan\theta_1 - \tan\theta_2} - \frac{x_2\tan\theta_1 - x_1\tan\theta_2 + (y_1 - y_2)\tan\theta_1\tan\theta_2}{(\tan\theta_1 - \tan\theta_2)^2}\right] \times \sec^2\theta_1,$$

$$\frac{\partial x_t}{\partial \theta_2} = \left[\frac{-x_1 + (y_1 - y_2)\tan\theta_1}{\tan\theta_1 - \tan\theta_2} + \frac{x_2\tan\theta_1 - x_1\tan\theta_2 + (y_1 - y_2)\tan\theta_1\tan\theta_2}{(\tan\theta_1 - \tan\theta_2)^2}\right] \times \sec^2\theta_2. \tag{9}$$

The last two partial derivatives could be rewritten using either the definition $\sec\theta = 1/\cos\theta$ or the identity $\sec^2\theta - \tan^2\theta = 1$. More importantly, we note $\partial x_t/\partial x_1 + \partial x_t/\partial x_2 = 1$ and $\partial x_t/\partial y_1 + \partial x_t/\partial y_2 = 0$. Thus while the individual error coefficients themselves have some dependence on the absolute coordinates, the appropriate pairs do not. Put another way, by appropriate choice of coordinates it is possible to reduce the sensitivity of the triangulation to errors in the x position of sensor 1, but only at the cost of an equal increase in the sensitivity to errors in the x position of sensor 2.

Performing a similar Taylor series expansion using Eq. (7), and again keeping only terms to first order, we can write the error propagation equation to first order for y_t:

$$\delta y_t \approx \frac{\partial y_t}{\partial y_1}\delta y_1 + \frac{\partial y_t}{\partial y_2}\delta y_2 + \frac{\partial y_t}{\partial x_1}\delta x_1 + \frac{\partial y_t}{\partial x_2}\delta x_2 + \frac{\partial y_t}{\partial \theta_1}\delta\theta_1 + \frac{\partial y_t}{\partial \theta_2}\delta\theta_2. \tag{10}$$

The various partial derivatives for this equation are

$$\frac{\partial y_t}{\partial y_1} = \frac{\tan\theta_1}{\tan\theta_1 - \tan\theta_2}, \qquad \frac{\partial y_t}{\partial y_2} = -\frac{\tan\theta_2}{\tan\theta_1 - \tan\theta_2},$$

$$\frac{\partial y_t}{\partial x_1} = \frac{-1}{\tan\theta_1 - \tan\theta_2}, \qquad \frac{\partial y_t}{\partial x_2} = \frac{1}{\tan\theta_1 - \tan\theta_2},$$

$$\frac{\partial y_t}{\partial \theta_1} = \left[\frac{y_1}{\tan\theta_1 - \tan\theta_2} - \frac{y_1\tan\theta_1 - y_2\tan\theta_2 + x_2 - x_1}{(\tan\theta_1 - \tan\theta_2)^2}\right]\sec^2\theta_1,$$

$$\frac{\partial y_t}{\partial \theta_2} = \left[\frac{-y_2}{\tan\theta_1 - \tan\theta_2} + \frac{y_1\tan\theta_1 - y_2\tan\theta_2 + x_2 - x_1}{(\tan\theta_1 - \tan\theta_2)^2}\right]\sec^2\theta_2. \tag{11}$$

Again we note that $\partial y_t/\partial x_1 + \partial y_t/\partial x_2 = 0$ and $\partial y_t/\partial y_1 + \partial y_t/\partial y_2 = 1$.

The first-order error propagation equation for the horizontal distance r_i between sensor i and the target t is given by

$$\delta r_i \approx \frac{\partial r_i}{\partial x_i}\delta x_i + \frac{\partial r_i}{\partial x_t}\delta x_t + \frac{\partial r_i}{\partial y_i}\delta y_i + \frac{\partial r_i}{\partial y_t}\delta y_t. \tag{12}$$

But for ∂x_t and ∂y_t in Eq. (12), we substitute Eqs. (8) and (10), yielding

$$\delta r_i \approx \frac{\partial r_i}{\partial x_i}\delta x_i + \frac{\partial r_i}{\partial x_t}\left(\frac{\partial x_t}{\partial x_1}\delta x_1 + \frac{\partial x_t}{\partial x_2}\delta x_2 + \frac{\partial x_t}{\partial y_1}\delta y_1 + \frac{\partial x_t}{\partial y_2}\delta y_2 + \frac{\partial x_t}{\partial \theta_1}\delta\theta_1 + \frac{\partial x_t}{\partial \theta_2}\delta\theta_2\right) + \frac{\partial r_i}{\partial y_i}\delta y_i + \frac{\partial r_i}{\partial y_t}\left(\frac{\partial y_t}{\partial y_1}\delta y_1 + \frac{\partial y_t}{\partial y_2}\delta y_2 + \frac{\partial y_t}{\partial x_1}\delta x_1 + \frac{\partial y_t}{\partial x_2}\delta x_2 + \frac{\partial y_t}{\partial \theta_1}\delta\theta_1 + \frac{\partial y_t}{\partial \theta_2}\delta\theta_2\right). \tag{13}$$

The remaining terms which must be evaluated are

$$\frac{\partial r_i}{\partial x_i}=\frac{x_i-x_t}{\sqrt{(x_i-x_t)^2+(y_i-y_t)^2}},$$

$$\frac{\partial r_i}{\partial x_t}=-\frac{x_i-x_t}{\sqrt{(x_i-x_t)^2+(y_i-y_t)^2}},$$

$$\frac{\partial r_i}{\partial y_i}=\frac{y_i-y_t}{\sqrt{(x_i-x_t)^2+(y_i-y_t)^2}}, \tag{14}$$

$$\frac{\partial r_i}{\partial y_t}=-\frac{y_i-y_t}{\sqrt{(x_i-x_t)^2+(y_i-y_t)^2}}.$$

Using the terms in Eqs. (9), (11), and (14), we can evaluate the error propagation equation (12) for the x-y plane distance between sensor i and the target t.

We are now ready to use Eq. (2) to write the first-order error propagation for z_t:

$$\delta z_t \approx \frac{\partial z_t}{\partial r_i}\delta r_i+\frac{\partial z_t}{\partial \varphi_i}\delta \varphi_i+\frac{\partial z_t}{\partial z_i}\delta z_i. \tag{15}$$

We have already computed δr_i. The remaining partial derivatives are

$$\frac{\partial z_t}{\partial r_i}=\tan\varphi_i,\quad \frac{\partial z_t}{\partial \varphi_i}=r_i\sec^2\varphi_i,\quad \frac{\partial z_t}{\partial z_i}=1. \tag{16}$$

At this point we have evaluated all the error propagation equations for x_t [Eq. (8)], y_t [Eq. (10)], r_i [Eq. (13)], and z_t [Eq. (15)]. The various partial derivatives required to evaluate these equations are contained in Eqs. (9), (11), (14), and (16). These can be easily programmed into a computer and evaluated for various sensor-to-target geometries.

We can make several observations about the propagation of measurement errors from the preceding equations.

1. The estimates of x_t and y_t are independent of any errors in measurement of either the sensor z position (z_i) or the elevation angle φ_i [from Eqs. (4), (6), (7)].
2. The errors in x_t and y_t arising from measurement errors in the sensor position (x_i, y_i) depend only on the azimuth angles (specifically, the angle between sensors) and not on the actual sensor (x,y) locations [Eqs. (9), (11)].
3. All of the partial derivatives for δx_t and δy_t [Eqs. (9) and (11)] contain $\tan\theta_1-\tan\theta_2$ in the denominator. This difference goes to zero, and hence the error propagation coefficients become infinite, when the two tangents are equal. This occurs when $\theta_1=\theta_2+k\pi$, for any integer k. The two cases of practical interest occur when $\theta_1=\theta_2$ and when $\theta_1=\theta_2+180$ deg.
4. Errors in the measurement of the z component of a sensor position translate directly into equivalent errors in the z component of the target position estimate [Eq. (16)].

2.3 *Error Propagation with Gaussian Statistics*

While Eq. (8) describes the error propagation from each independent variable to the final estimate of x_t, most measurement errors can be described by a random, Gaussian error process. In this case, we can derive an estimate of the standard deviation of the estimated target position (x_t) by squaring Eq. (8), taking the expectation value, and finally taking the square root. Assuming the errors are not correlated, the result is

$$\sigma_{x_t}\approx\left[\left(\frac{\partial x_t}{\partial x_1}\sigma_{x_1}\right)^2+\left(\frac{\partial x_t}{\partial x_2}\sigma_{x_2}\right)^2+\left(\frac{\partial x_t}{\partial y_1}\sigma_{y_1}\right)^2+\left(\frac{\partial x_t}{\partial y_2}\sigma_{y_2}\right)^2+\left(\frac{\partial x_t}{\partial \theta_1}\sigma_{\theta_1}\right)^2+\left(\frac{\partial x_t}{\partial \theta_2}\sigma_{\theta_2}\right)^2\right]^{1/2}, \tag{17}$$

where σ_a is the standard deviation in measurements for the variable a. This equation summarizes the fact that, in general, measurement errors in independent variables are not correlated and hence do not always add with the same sign. Extension of Eq. (17) to the case in which two of the variables are correlated is straightforward. If two variables (v_1 and v_2) are correlated, the expectation value of the cross term $\langle \delta v_1\, \delta v_2\rangle$ will be nonzero with value $\rho\sigma_{v1}\sigma_{v2}$, where $-1\leqslant\rho\leqslant 1$. This will lead to an additional term within the square root, of the form $2(\partial x_t/\partial v_1)\times(\partial x_t/\partial v_2)\rho\sigma_{v1}\sigma_{v2}$.

Similarly, we can use Eq. (10) to derive an estimate of the standard deviation of y_t:

$$\sigma_{y_t}\approx\left[\left(\frac{\partial y_t}{\partial x_1}\sigma_{x_1}\right)^2+\left(\frac{\partial y_t}{\partial x_2}\sigma_{x_2}\right)^2+\left(\frac{\partial y_t}{\partial y_1}\sigma_{y_1}\right)^2+\left(\frac{\partial y_t}{\partial y_2}\sigma_{y_2}\right)^2+\left(\frac{\partial y_t}{\partial \theta_1}\sigma_{\theta_1}\right)^2+\left(\frac{\partial y_t}{\partial \theta_2}\sigma_{\theta_2}\right)^2\right]^{1/2}. \tag{18}$$

Equation (13) yields

$$\begin{aligned}\sigma_{r_i}^2\approx&\left(\frac{\partial r_i}{\partial x_i}\right)^2\sigma_{x_i}^2+\left(\frac{\partial r_i}{\partial y_i}\right)^2\sigma_{y_i}^2+\left(\frac{\partial r_i}{\partial x_t}\right)^2\left[\left(\frac{\partial x_t}{\partial x_1}\right)^2\sigma_{x_1}^2\right.\\&+\left(\frac{\partial x_t}{\partial x_2}\right)^2\sigma_{x_2}^2+\left(\frac{\partial x_t}{\partial y_1}\right)^2\sigma_{y_1}^2+\left(\frac{\partial x_t}{\partial y_2}\right)^2\sigma_{y_2}^2+\left(\frac{\partial x_t}{\partial \theta_1}\right)^2\sigma_{\theta_1}^2\\&\left.+\left(\frac{\partial x_t}{\partial \theta_2}\right)^2\sigma_{\theta_2}^2\right]+\left(\frac{\partial r_i}{\partial y_t}\right)^2\left[\left(\frac{\partial y_t}{\partial y_1}\right)^2\sigma_{y_1}^2+\left(\frac{\partial y_t}{\partial y_2}\right)^2\sigma_{y_2}^2\right.\\&+\left(\frac{\partial y_t}{\partial x_1}\right)^2\sigma_{x_1}^2+\left(\frac{\partial y_t}{\partial x_2}\right)^2\sigma_{x_2}^2+\left(\frac{\partial y_t}{\partial \theta_1}\right)^2\sigma_{\theta_1}^2\\&\left.+\left(\frac{\partial y_t}{\partial \theta_2}\right)^2\sigma_{\theta_2}^2\right].\end{aligned} \tag{19}$$

Finally, Eq. (15) gives [with the substitution of $\partial z_t/\partial z_i=1$, from equation (16)]

$$\sigma_{z_t} \approx \left[\left(\frac{\partial z_t}{\partial r_i} \right)^2 \sigma_{r_i}^2 + \left(\frac{\partial z_t}{\partial \varphi_i} \right)^2 \sigma_{\varphi_i}^2 + \sigma_{z_i}^2 \right]^{1/2}. \tag{20}$$

To proceed from here, we make the assumption that the standard deviations of measurement errors for sensors 1 and 2 are independent of the sensor, and hence equal. We further assume that there is no preferred direction, and hence measurement errors of the sensor position will have the same standard deviations in the x and the y direction. These two assumptions can be written

$$\sigma_{x_1} = \sigma_{x_2} = \sigma_{y_1} = \sigma_{y_2} \equiv \sigma_{\text{pos}}, \quad \sigma_{\theta_1} = \sigma_{\theta_2} \equiv \sigma_\theta. \tag{21}$$

Using these assumptions, we can rewrite Eqs. (17), (18), and (19) as follows [Eq. (20) remains unchanged]:

$$\sigma_{x_t} \approx \left\{ \left[\left(\frac{\partial x_t}{\partial x_1} \right)^2 + \left(\frac{\partial x_t}{\partial x_2} \right)^2 + \left(\frac{\partial x_t}{\partial y_1} \right)^2 + \left(\frac{\partial x_t}{\partial y_2} \right)^2 \right] \sigma_{\text{pos}}^2 + \left[\left(\frac{\partial x_t}{\partial \theta_1} \right)^2 + \left(\frac{\partial x_t}{\partial \theta_2} \right)^2 \right] \sigma_\theta^2 \right\}^{1/2}, \tag{22}$$

$$\sigma_{y_t} \approx \left\{ \left[\left(\frac{\partial y_t}{\partial x_1} \right)^2 + \left(\frac{\partial y_t}{\partial x_2} \right)^2 + \left(\frac{\partial y_t}{\partial y_1} \right)^2 + \left(\frac{\partial y_t}{\partial y_2} \right)^2 \right] \sigma_{\text{pos}}^2 + \left[\left(\frac{\partial y_t}{\partial \theta_1} \right)^2 + \left(\frac{\partial y_t}{\partial \theta_2} \right)^2 \right] \sigma_\theta^2 \right\}^{1/2}, \tag{23}$$

$$\begin{aligned} \sigma_{r_i}^2 \approx & \left\{ \left(\frac{\partial r_i}{\partial x_i} \right)^2 + \left(\frac{\partial r_i}{\partial y_i} \right)^2 + \left(\frac{\partial r_i}{\partial x_t} \right)^2 \left[\left(\frac{\partial x_t}{\partial x_1} \right)^2 + \left(\frac{\partial x_t}{\partial x_2} \right)^2 + \left(\frac{\partial x_t}{\partial y_1} \right)^2 + \left(\frac{\partial x_t}{\partial y_2} \right)^2 \right] + \left(\frac{\partial r_i}{\partial y_t} \right)^2 \left[\left(\frac{\partial y_t}{\partial y_1} \right)^2 + \left(\frac{\partial y_t}{\partial y_2} \right)^2 \right. \right. \\ & \left. \left. + \left(\frac{\partial y_t}{\partial x_1} \right)^2 + \left(\frac{\partial y_t}{\partial x_2} \right)^2 \right] \right\} \sigma_{\text{pos}}^2 + \left\{ \left(\frac{\partial r_i}{\partial x_t} \right)^2 \left[\left(\frac{\partial x_t}{\partial \theta_1} \right)^2 + \left(\frac{\partial x_t}{\partial \theta_2} \right)^2 \right] + \left(\frac{\partial r_i}{\partial y_t} \right)^2 \left[\left(\frac{\partial y_t}{\partial \theta_1} \right)^2 + \left(\frac{\partial y_t}{\partial \theta_2} \right)^2 \right] \right\} \sigma_\theta^2. \end{aligned} \tag{24}$$

Equation (20) provides an error estimate for z_t from a single sensor. Since we have two sensors, we compute an estimate of z_t from each sensor and then average them [weighted by their standard deviation given in Eq. (20)] to obtain our best estimate of z_t [Eq. (5)]. Since both estimates of z_t depend on the position and pointing parameters of both sensors (through r_i), the error estimate [using Eq. (15)] becomes

$$\langle \sigma_{z_t} \rangle = \frac{1}{2} \left[\sigma_{z_t}^2(1) + \sigma_{z_t}^2(2) + 2 \frac{\partial z_t}{\partial r_1} \frac{\partial z_t}{\partial r_2} \text{Cov}(\delta r_1, \delta r_2) \right]^{1/2}, \tag{25}$$

where $\sigma_z(1)$ is the result obtained from Eq. (20) for sensor 1, while $\sigma_z(2)$ is the result obtained for sensor 2. The two partial derivatives are given by Eq. (16) as simply the tangents of the elevation angles of the respective sensors. We evaluate the covariance $\text{Cov}(\delta r_1, \delta r_2)$ as the expectation value of the product $\langle \delta r_1 \, \delta r_2 \rangle$. After much algebra, we arrive at

$$\text{Cov}(\delta r_1, \delta r_2) = \frac{\partial r_1}{\partial x_t} \frac{\partial r_2}{\partial x_t} \sigma_{x_t}^2 + \frac{\partial r_1}{\partial y_t} \frac{\partial r_2}{\partial y_t} \sigma_{y_t}^2. \tag{26}$$

The partial derivatives are given in Eqs. (14), while expressions for the standard deviations are given by Eqs. (22) and (23).

Equations (20) to (26) are our final error propagation equations relating the standard deviation of our measurement errors to errors in the final target location estimation. For a two-sensor system, we can use equations (3) and (5) to (7) to compute an estimate of the target location (x_t, y_t, z_t). Then we can use Eqs. (20) to (26) to provide error estimates for those values, based on estimates of the measurement errors.

3 Results

3.1 *Methodology*

In this section we numerically examine the effect of sensor location and pointing errors on estimates of target location. This is done by examining the behavior of the coefficients of the sensor position errors (σ_{pos}) and sensor azimuth errors (σ_θ) in the equations for target location (x_t, y_t) and sensor-to-target range r_i [Eqs. (22) to (24)]. We also examine the behavior of the coefficient of the sensor elevation angle σ_φ on estimates of the target z_t location [Eq. (20)]. It turns out that the dominant effects are the sensor azimuth separation angle $(\theta_1 - \theta_2)$, the range to the target, and the sensor elevation angle.

In order to compute these coefficients, each of the partial derivatives in Eqs. (9), (11), (14), and (16) was coded in a computer program. The accuracy of the computer implementation was checked by comparing the results for several sets of known inputs against hand calculations performed directly from the equations. Another check involved comparing the values of the partial derivatives with the difference between the known and computed target location when a known error was introduced into Eqs. (2), (4), (6), and (7). A further check of the implementation was performed by plotting several of the partial-derivative pairs, such as $\partial x_t / \partial x_1 + \partial x_t / \partial x_2$, versus the azimuth angle between sensor 1 and sensor 2 $(\theta_1 - \theta_2)$ and checking that they gave the appropriate constant value (e.g., 1 or 0) for all separation angles.

Once the validity of the computer implementation of the partial derivatives was assured, the error coefficients for the measurement errors in Eqs. (20) and (22) to (24) were coded. Again, these were checked against hand calculations using the values of the partial derivatives as input.

To generate the plots in the next section, a computer simulation was developed in which a target is placed at coordinates $x_t = 50$, $y_t = 100$, $z_t = 2$ $(50, 100, 2)$. Next, a sensor 1 azimuth angle θ_1, range r_1, and z-axis position z_1 are selected. In most cases, a range of 5 units was used. Using this information, the (x_1, y_1) coordinates of sensor 1 and the elevation angle φ_1 are determined. Next, sensor 2 is placed at the same range $(r_1 = r_2)$, but is moved in 1-deg increments around the target, so that the azimuth separation $\theta_2 - \theta_1$ varies between 1 and 179 deg. At each increment, the error propagation coefficients are computed. This was

typically done for a variety of different sensor 1 azimuth angles. The coefficients of σ_{pos} measurement errors are in units of target position error per unit of sensor location error. The coefficients of σ_θ measurement errors are in units of target position error per degree of sensor azimuth error.

In order to determine the (x,y) coordinates of each sensor, given the range and the azimuth angle to the target, Eqs. (1) and (3) were solved for $\Delta x = |x_t - x_i|$ and $\Delta y = |y_t - y_i|$. The results are

$$\Delta y_i = \left(\frac{r_i^2}{\tan^2 \theta_i + 1} \right)^{1/2}, \tag{27}$$

$$\Delta x_i = (r_i^2 - \Delta y_i^2)^{1/2}, \tag{28}$$

$$\tan \varphi_i = \frac{\Delta z_i}{r_i}. \tag{29}$$

The next subsection, giving the explicitly computed error propagation graphs, is followed by a subsection containing Monte Carlo results for several different sensor pair configurations. Four sensors are used to generate six pairs of sensors. All four sensors are located at a range of 5 units from the target. Sensor 1 is located at an azimuth angle of 40 deg, sensor 2 at 50 deg, sensor 3 at 130 deg, and sensor 4 at 140 deg. This allows two sensor pairs at 10-deg separation, one pair at 80-deg separation, two pairs at 90-deg separation, and one pair at 100-deg separation.

Equations (6), (7), and (3) are used to compute the target x-y location and the sensor-1-to-target range for each pair of sensors. One thousand sample runs were used, having Gaussian-distributed measurement errors. The standard deviation of the target x-y position estimate and of the sensor-1-to-target range estimate was computed for each sensor pair. The results are compared with the analytical predictions in the graphs (Sec. 3.2).

3.2 *Error Propagation Graphs*

We begin by examining the behavior of the coefficients of σ_{pos} and σ_θ in Eqs. (22) and (23). Figures 2–5 show plots of the coefficients as a function of the azimuth angle between the sensors $(\theta_1 - \theta_2)$. As can be seen from Eqs. (9) and (11), these coefficients depend not only on the azimuth angle between sensors, but also on the absolute azimuth angle. We examine this dependence by selecting various fixed sensor 1 azimuth angles (θ_1) and then varying the sensor 2 azimuth angle (θ_2).

Examining Figs. 2 and 3, showing the sensitivity of x and y target position estimates to sensor location measurement errors as functions of azimuth separation angle, we see that, as one might expect, they are equivalent, with a 90-deg shift in θ_1 values between the two graphs. In both cases, minimum sensitivity is obtained at an azimuth separation angle of 90 deg. The target position sensitivity to sensor position measurement error varies from 1:1 at a 90-deg separation angle to 4 : 1 at 20- and 160-deg separation angles.

Examining Figs. 4 and 5, showing the sensitivities of x and y target position estimates to sensor azimuth measurement errors (in degrees) as functions of azimuth separation angle, we see that, as one might expect, they are equivalent, with a 90-deg shift in θ_1 values between the two graphs. In both cases, minimum sensitivity is obtained at an azimuth separation angle of 90 deg. The target position sensitivity to sensor azimuth measurement error varies from 0.087:1 at a 90-deg separation angle to 0.35:1 at 20- and 160-deg separation angles. This means that at a 90-deg separation angle, a 1-deg azimuth measurement error will result in a 0.087-unit target position error.

From Eqs. (9), (11), (22), and (23), we can see that the coefficients for σ_{pos} do not depend on sensor location and hence have no range dependence. However, the coefficients for σ_θ do depend on the sensor locations and hence do have a range dependence. A plot (not shown, to conserve space) of the coefficients of σ_θ in Eqs. (22) and (23) shows an exact one-to-one scaling with range. Thus the coefficient of σ_θ in Eqs. (22) and (23), for a range of $2r$, is equal to twice

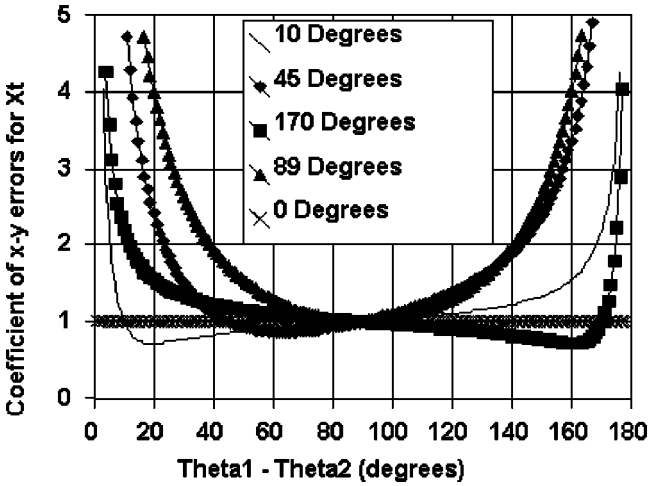

Fig. 2 Coefficient of σ_{pos} in Eq. (22) for σ_x as a function of azimuth separation angle $\theta_1 - \theta_2$ for various values of sensor 1 azimuth angle θ_1.

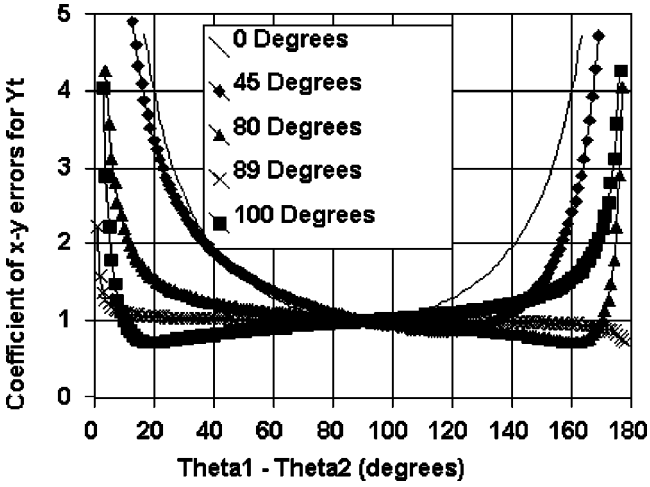

Fig. 3 Coefficient of σ_{pos} in Eq. (23) for σ_y as a function of azimuth separation angle $\theta_1 - \theta_2$ for various values of sensor 1 azimuth angle θ_1.

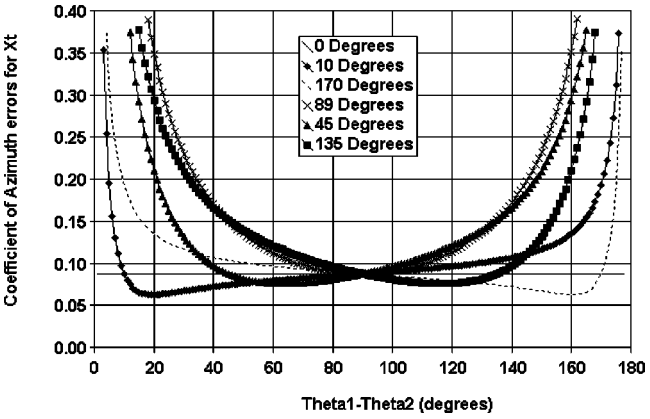

Fig. 4 Coefficient of σ_θ in Eq. (22) for σ_x as a function of azimuth separation angle $\theta_1-\theta_2$ for various values of sensor 1 azimuth angle θ_1. Sensor-to-target range is 5 units. Coefficient is for azimuth errors measured in degrees.

the coefficient at a range of r [coeff:$\sigma_\theta(2r)$ $=2$ coeff:$\sigma_\theta(r)$]. The plots of the σ_θ coefficients (Figs. 4 and 5) are for a range of 5 units. Thus to scale to other ranges, one would divide by 5 and multiply by the appropriate range.

Errors in our estimation of the sensor to target range [σ_r, Eq. (24)] affect the accuracy of our estimate of the target z location [σ_z, Eq. (20)]. Equation (24) describes how the error measurements in the sensor locations and azimuth angles are related to the estimate of the sensor to target range. The coefficient of σ_{pos} (range error as a function of sensor location error) is independent of the target-to-sensor range and almost independent of absolute angle, exhibiting only a dependence on the angle between sensors (Fig. 6). The coefficient of σ_θ (range error as a function of sensor azimuth angle error) is almost independent of absolute angle, but has a direct linear scaling with range. Figure 7 shows a plot of the coefficient of σ_θ (for azimuth errors in degrees) as a function of azimuth separation angle for a range of 5 units.

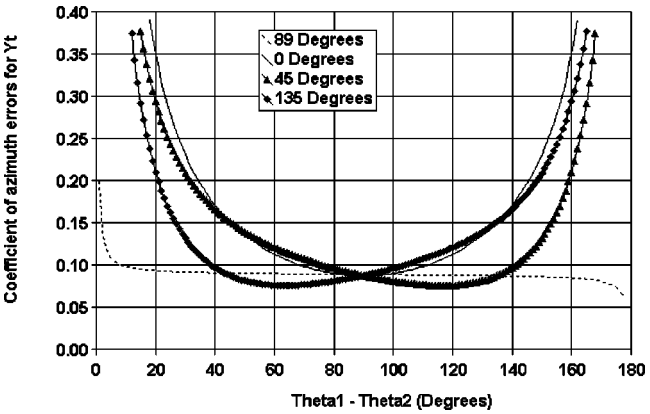

Fig. 5 Coefficient of σ_θ in Eq. (23) for σ_y as a function of azimuth separation angle $\theta_1-\theta_2$ for various values of sensor 1 azimuth angle θ_1. Sensor-to-target range is 5 units. Coefficient is for azimuth errors in degrees.

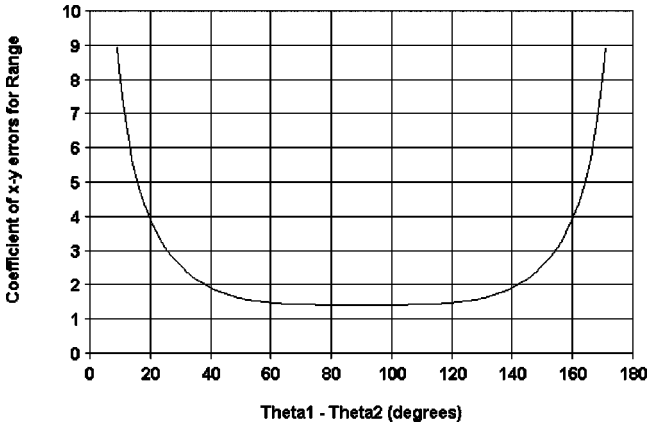

Fig. 6 Coefficient of σ_{pos} in Eq. (24) for σ_r as a function of azimuth separation angle $\theta_1-\theta_2$.

From Fig. 6 we see a broad flat region of minimum sensitivity of 1.4:1 between separation angles of 60 and 120 deg. The sensitivity then increases to 4:1 at angles of 20 and 160 deg. From Fig. 7 we see that the range sensitivity to azimuth measurement errors varies between 0.087:1 at a separation angle of 90 deg and 0.33 range units per degree of azimuth error at separation angles of 20 and 160 deg (at a range of 5 units).

Next we examine the behavior of the coefficients of σ_r and σ_φ in Eq. (20). As given by Eq. (16), the coefficient of σ_φ is $\partial z_t/\partial\varphi_i = r_i \sec^2\varphi_i$. This obviously scales linearly with sensor-to-target range r_i. A plot of this coefficient (in units per degree) as function of φ_i, for fixed range (5 units), is shown in Fig. 8. The coefficient of σ_r is simply $\partial z_t/\partial r_i = \tan\varphi_i$, as given by Eq. (16). Since this can be looked up in many standard references, or computed trivially, the graph is omitted in order to save space.

3.3 *Monte Carlo Results*

The first set of 1000 runs was performed using a sensor position measurement error with a standard deviation of 1.0 unit. A separate set of random numbers was generated for both the x and the y sensor location for each sensor. The

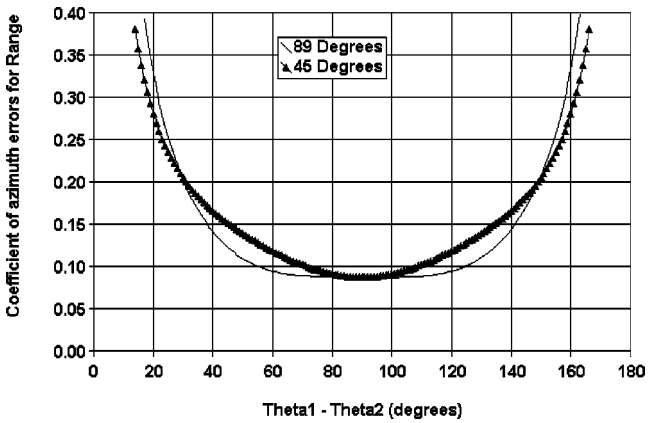

Fig. 7 Coefficient of σ_θ in Eq. (24) for σ_r as a function of azimuth separation angle $\theta_1-\theta_2$. Sensor-to-target range is 5 units. Coefficient is for azimuth errors in degrees.

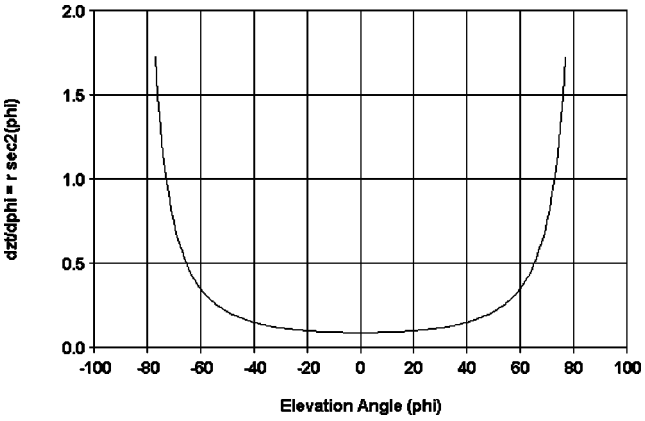

Fig. 8 Coefficient of σ_φ in Eq. (20) as a function of elevation angle φ for a sensor-to-target range of 5 units. Coefficient is for elevation errors in degrees.

second set of 1000 runs was performed using a sensor azimuth angle measurement error with a standard deviation of 1 deg. A separate set of random numbers was generated for each sensor. As already mentioned, all four sensors were at a range of 5 units from the target, but with azimuth angles of 40, 50, 130, and 140 deg. Table 1 gives the standard deviation of the target location (x,y) and sensor-1-to-target range for the first set of runs (sensor position measurement error). Table 2 gives the same information for the second set of runs (sensor azimuth angle measurement errors).

We can compare the Monte Carlo results presented here with the predictions of the analytically computed graphs in the last section. If we compare line 2 (sensor pair 1 and 3, 90-deg separation, $\theta_1 = 40$ deg), in both tables, with the graphs, we find excellent agreement. At a separation of 90 deg, Figs. 2 and 3 predict a standard deviation for both x and y of 1, compared to Table 1 values of 1.00 and 0.96. Figures 3 and 4 predict a standard deviation for both x and y of about 0.087, compared to Table 2 values of 0.087 and 0.088. Similar comparisons can be made for σ_r using Figs. 6 and 7. We can compare the line 1 (sensor pair 1 and 2, 10-deg separation, $\theta_1 = 40$ deg) with the graphs using the $\theta_1 = 45$-deg data set as an approximation. Again good agreement is found in all cases.

4 Discussion

In this section, we summarize what we have learned and then apply it to two cases: (1) a laboratory application and (2) a test-range application.

Table 1 Sensor position measurement error; standard deviation = 1.0 unit.

Sensors	Angles (deg)	σ_x	σ_y	σ_r
1, 2	40, 50	5.74	5.73	5.70
1, 3	40, 130	1.00	0.96	1.41
1, 4	40, 140	0.93	1.08	1.50
2, 3	50, 130	1.07	0.90	1.44
2, 4	50, 140	0.99	0.99	1.43
3, 4	130, 140	5.68	5.66	5.65

Table 2 Sensor azimuth measurement error; standard deviation = 1.0 deg.

Sensors	Angles (deg)	σ_x	σ_y	σ_r
1, 2	40, 50	0.555	0.555	0.780
1, 3	40, 130	0.087	0.088	0.088
1, 4	40, 140	0.079	0.097	0.091
2, 3	50, 130	0.095	0.081	0.090
2, 4	50, 140	0.086	0.089	0.088
3, 4	130, 140	0.554	0.551	0.776

The basic equations for estimating target position in three dimensions (x,y,z) are given in Sec. 2.1. The target (x,y) position can be estimated using either Eq. (4) for an N-sensor problem, or Eqs. (6) and (7) when using two sensors at a time. From this result, one estimates the horizontal sensor-to-target range for each sensor, using Eq. (3). Finally, one estimates the target z location, using Eq. (5).

Section 2.2 develops the basic error propagation equations, which allow one to determine the effect on the position estimate resulting from specific errors in the sensor location and pointing measurements. Equations (8) to (11) give the error propagation equations and coefficients for estimates of the target (x,y) location. Equations (13), (14) give the error propagation equation and coefficients for estimates of the sensor-to-target range, and Eqs. (15), (16) give the error propagation equations and coefficients for estimates of the target z location.

While Sec. 2.2 allows one to determine the effect of a specific measurement error on the target position estimate, Sec. 2.3 introduces Gaussian measurement error and allows one to relate the standard deviation in sensor location and orientation measurements to a standard deviation in the target location estimate. In this model, there are three measurement uncertainties: the standard deviation of sensor (x,y) location measurements, σ_{pos}; the standard deviation of sensor azimuth measurements, σ_θ; and the standard deviation of sensor elevation angle measurements, σ_φ. Given these uncertainties, and approximate sensor locations, azimuth angles, and elevation angles, one can estimate the standard deviation of the target position estimates using Eqs. (22) to (24) and (20).

Section 3.2 presents graphs of the error propagation coefficients relating the standard deviation of measurement errors to the standard deviation of target position estimates [from Eqs. (20) to (24)]. Examining Figs. 2–7, we see that estimates of the target (x,y) location, and hence sensor-to-target range, have a strong dependence on the azimuth angle between sensors, with a minimum error propagation occurring at an angular separation of 90 deg. In general, the error propagation curves become steeper as the sensor-to-sensor azimuth separation decreases below 90 deg or increases above 90 deg, becoming infinite at 0 and 180 deg. As a general rule of thumb, the curves appear to be relatively flat between 60 and 120 deg, thus providing a preferred range of orientations. The curves become quite steep for separations less than 20 and greater than 160 deg, indicating that orientations in these ranges are to be avoided. Another interesting observation is the sensitivity to the ab-

solute sensor orientation shown in Figs. 2 to 5. What this sensitivity indicates is that one can minimize the sensitivity of either the x or the y target location (to sensor location and orientation errors), at the expense of increased sensitivity in the other dimension.

While the coefficients of sensor location measurement errors (Figs. 2, 3, 6) depend primarily on sensor-to-sensor azimuth separation angle, and not on sensor-to-target range, the coefficients of sensor azimuth angle measurement errors (Figs. 4, 5, 7) depend linearly on the range. The figures shown here are for a range of 5 units. To apply these graphs, they must be scaled by the appropriate range. Thus divide by 5 and multiply by the sensor-to-target range in your system of units. Reading from the graphs, at a separation angle of 90 deg, there is a 1:1 relation between sensor location measurement errors and target position estimation, while there is a 0.087-unit error per degree of azimuth angle error (at a range of 5 units).

Finally, Fig. 8 shows the sensitivity of the target z position estimate to errors in the measurement of the sensor elevation angle. The sensitivity is relatively flat between elevation angles of -40 and $+40$ deg with a minimum at 0-deg elevation. The sensitivity increases rapidly at elevation angles below -60 and above $+60$ deg.

Section 3.3 uses a Monte Carlo approach to numerically verify the error coefficients derived in Sec. 2.3 and graphed in Sec. 3.2. Very good agreement is obtained, thus giving confidence in the mathematical formulation and the software implementation, as expressed in the graphical results. This independent validation gives confidence that the graphical results of Sec. 3.2 are correct.

We now turn to the two example cases (laboratory and test range), in order to demonstrate how to utilize the results of this paper in a practical application. For a typical automotive crash test application, one might want to measure a 3D position to an accuracy of 5 mm, using two sensors at a range of 4 m from the target area. One is typically constrained on the sensor separation, so we will assume a sensor azimuth separation of 40 deg. Referring to Fig. 2, if sensor 1 has an azimuth angle of 45 deg to the target, then for the 40-deg separation, our error propagation coefficient for the target x position for sensor position errors is 1.11. Similarly, for the target y position, the coefficient is 1.90. The error coefficient for azimuth errors is $0.097\times 4/5 = 0.078$ m/deg for the x measurement and $0.166\times 4/5 = 0.133$ m/deg for the y measurement. The ratio 4/5 is to scale the range from the 5-unit range used in this paper to the 4-m range in the example. If we divide our error equally between location measurement and azimuth measurement (allocating 2.5 mm of error to each), then we need to measure the sensor location to 1.3 mm (2.5 mm/1.90) accuracy in the laboratory frame of reference. We need to measure the azimuth pointing angle to 0.02 deg$=0.35$ mrad [(0.0025 m)/(0.133 m/deg)]. If we use a 512×512-pixel sensor with a 20-deg field of view, then the IFOV (pixel field of view) is 0.04 deg. This implies we need to measure target locations to better than $\frac{1}{2}$-pixel accuracy. The preceding sensor location and pointing accuracy requirements are those necessary to compute an absolute 3D position for the target. If, on the other hand, one only needs to compute target position relative to other objects in the field of view, then accuracy of the absolute sensor location and pointing angle is not important (as long as the sensor is stationary). However, the pixel accuracy requirement still obtains.

For a range application, one may use a tracking mount, as opposed to a static mount with fixed pointing. A typical accuracy might be 2 m at a range of 5 km. In this case, we might assume a 0.25-deg field of view with a 512×512 sensor, giving 1.76 arcsec per pixel, or 8.5 μrad per pixel. For this example, we will assume an optimal 90-deg azimuth separation angle. The coefficient of sensor location measurement errors (Figs. 2, 3) is 1.0, while the coefficient of azimuth angle measurement errors is $0.087\times(5/5) = 0.087$ km per degree of error (Figs. 4, 5). Again dividing the errors equally between sensor location and azimuth angle errors, we see that we must know the sensor position to an accuracy of 1 m (quite doable with differential GPS technology). We must know our azimuth pointing angles to an accuracy of $(1\text{ m})/(87\text{ m/deg}) = 0.01\text{deg} = 17$ μrad. The estimate of the target z position depends on the sensor z location measurement, the accuracy of the sensor elevation angle measurement, and the accuracy of the sensor-to-target range. If we assume a 40-deg elevation angle, then from Fig. 8, the elevation angle error coefficient is 0.2 km/deg. Thus we need to know the elevation angle to 0.005 deg to have 1-m accuracy.

5 Conclusions

This paper has developed the error propagation equations for use with two angles-only sensors to perform a 3D position estimation via triangulation. The analytical error propagation equations developed in Sec. 2 and graphed in Sec. 3.2 have been verified using a Monte Carlo approach in Sec. 3.3.

The optimum geometry for a two-sensor system is to have a 90-deg azimuth separation angle between the two sensors. The target (x,y) position estimation accuracy depends on the accuracy of the sensor location measurement, the sensor azimuth pointing measurement, the sensor-to-target range, and the sensor-to-sensor azimuth separation geometry. The target z position estimation accuracy depends on the sensor-to-target horizontal range [and hence all of the preceding components of the (x,y) position estimation], the sensor z location measurement accuracy, and the sensor elevation angle measurement.

The equations and graphs in this paper give practical tools for designing a two-sensor 3D position estimation system to achieve a desired level of accuracy. They are also useful for estimating the accuracy of an existing system. Future work should extend the current analysis to a full multisensor (more than two) system.

References

1. D. E. Manolakis, ''Efficient solution and performance analysis of 3-D position estimation by trilateration,'' *IEEE Trans. Aerosp. Electron. Syst.* **32**(4), 1239–1248 (1996).
2. D. E. Manolakis and M. E. Cox, ''Effect in range difference position estimation due to stations position errors,'' *IEEE Trans. Aerosp. Electron. Syst.* **34**(1), 329–334 (1998).
3. W. Navidi, W. S. Murphy, and W. Hereman, ''Statistical methods in surveying by trilateration,'' *Comput. Stat. Data Anal.* **27**(2), (1998).
4. H. C. Harris, C. C. Dahn, D. G. Monet, and J. R. Pier, ''Trigonometric parallaxes of planetary-nebulae,'' *IAU Symp.* **180**, 40–45 (1997).
5. C. C. Dahn, ''Review of CCD parallax measurements,'' *IAU Symp.* **189**, 19–24 (1997).
6. V. V. Makarov, ''Absolute measurements of trigonometric parallaxes

with astrometric satellites,'' *Astron. Astrophys.* **340**(1), 309–314 (1998).
7. S. J. Ratcliff, T. J. Balonek, L. A. Marschall, D. L. Dupuy, C. R. Pennypacker, R. Verma, A. Alexov, and V. Bonney, ''The measurement of astronomical parallaxes with CCD imaging cameras on small telescopes,'' *Am. J. Phys.* **61**(3), 208–216 (1993).
8. F. H. Hollister, ''Bearings-only passive ranging using Kalman-Bucy and Moore-Penrose methods,'' *Proc. SPIE* **302**, 152–157 (1981).
9. J. R. Guerci, R. A. Goetz, and J. DiModica, ''A method for improving extended Kalman filter performance for angle-only passive ranging,'' *IEEE Trans. Aerosp. Electron. Syst.* **30**(4), 1090–1093 (1994).
10. H. H. Kagiwada, J. K. Kagiwada, and R. E. Kalaba, ''Precision passive ranging,'' *Comput. Math. Appl.* **26**(4), 89–96 (1993).
11. Y. G. Guezennec, R. S. Brodkey, N. Trigui, and J. C. Kent, ''Algorithms for fully automated three-dimensional particle tracking velocimetry,'' *Exp. Fluids* **17**, 209–219 (1994).
12. A. A. Adamczyk and L. Rimain, ''Reconstruction of a 3-dimensional flow field from orthogonal views of seed track video images,'' *Exp. Fluids* **6**, 380–386 (1988).
13. R. G. Racca and J. M. Dewey, ''A method for automatic particle tracking in a three-dimensional flow field,'' *Exp. Fluids* **6**, 25–32 (1988).
14. J. C. Kent, N. Trigui, W-C. Choi, Y. G. Guezennec, and R. S. Brodkey, ''Photogrammetric calibration for improved three-dimensional particle tracking velocimetry (3-D PTV),'' *Proc. SPIE* **2005**, 400–412 (1993).
15. N. Kasagi and K. Nishino, ''Probing turbulence with three-dimensional particle-tracking velocimetry,'' *Exp. Therm. Fluid Sci.* **4**, (1991).
16. W-C. Choi, Y. G. Guezennec, and R. S. Brodkey, ''In situ calibration and stereo matching for 3-D particle image velocimetry,'' *Bull. Am. Phys. Soc.* **36**, (1992).
17. T. P. K. Chang, A. T. Watson, and G. B. Tatterson, ''Image processing of tracer particle motions as applied to mixing and turbulent flow,'' *Chem. Eng. Sci.* **40**(2), 269–275 (1985).
18. Y. G. Guezennec and N. Kiritsis, ''Statistical investigation of errors in particle image velocimetry,'' *Exp. Fluids* **10**, 138–146 (1990).
19. J. E. Angus, ''Some consequences of sensor error in a model for passive detection,'' *Math. Comput. Modell.* **18**(2), 1–7 (1993).
20. J. N. Sanders-Reed, ''Vehicle real-time attitude estimation system (VRAES),'' *Proc. SPIE* **2739**, 266–277 (1996).
21. B. Sridhar and R. Suorsa, ''Comparison of motion and stereo methods in passive ranging systems,'' *IEEE Trans. Aerosp. Electron. Syst.* **27**(4), 741–746 (1991).

John N. Sanders-Reed is group leader for the Algorithms & Analysis group at Boeing-SVS, Inc. In this capacity he has led a number of development projects, including real-time trackers, remote sensing data acquisition and analysis for over 100 Gbyte of image data per day, and various stereo imaging projects. He is the developer of the Visual Fusion motion analysis software package, which performs multisensor 3D position and orientation estimation. Prior to joining Boeing-SVS, Dr. Sanders-Reed worked for 5 years at MIT Lincoln Laboratory, developing missile flight analysis software and maximum-likelihood space surveillance algorithms. Prior to that he worked for 5 years at Picker International, developing the first laser film recorder in the medical industry and developing theory for dual energy digital radiography. Dr. Sanders-Reed earned a PhD in physics from Case Western Reserve University and an MBA in high technology from Northeastern University. He has published over a dozen technical papers in the areas of medical imaging, surface science, image processing, and tracking.